Commun. Comput. Phys.
doi: 10.4208/cicp.070110.020710a

Vol. **10**, No. 1, pp. 161-182
July 2011

A Tailored Finite Point Method for Solving Steady MHD Duct Flow Problems with Boundary Layers

Po-Wen Hsieh[1], Yintzer Shih[2] and Suh-Yuh Yang[1,*]

[1] *Department of Mathematics, National Central University, Jhongli City, Taoyuan County 32001, Taiwan.*
[2] *Department of Applied Mathematics, National Chung Hsing University, Taichung 40227, Taiwan.*

Received 7 January 2010; Accepted (in revised version) 2 July 2010

Available online 30 March 2011

Abstract. In this paper we propose a development of the finite difference method, called the tailored finite point method, for solving steady magnetohydrodynamic (MHD) duct flow problems with a high Hartmann number. When the Hartmann number is large, the MHD duct flow is convection-dominated and thus its solution may exhibit localized phenomena such as the boundary layer. Most conventional numerical methods can not efficiently solve the layer problem because they are lacking in either stability or accuracy. However, the proposed tailored finite point method is capable of resolving high gradients near the layer regions without refining the mesh. Firstly, we devise the tailored finite point method for the scalar inhomogeneous convection-diffusion problem, and then extend it to the MHD duct flow which consists of a coupled system of convection-diffusion equations. For each interior grid point of a given rectangular mesh, we construct a finite-point difference operator at that point with some nearby grid points, where the coefficients of the difference operator are tailored to some particular properties of the problem. Numerical examples are provided to show the high performance of the proposed method.

AMS subject classifications: 65N06, 65N12, 76W05

Key words: Magnetohydrodynamic equations, Hartmann numbers, convection-dominated problems, boundary layers, tailored finite point methods, finite difference methods.

1 Introduction

The purpose of this paper is to devise an efficient tailored finite point method for approximating the solution of magnetohydrodynamic (henceforth, MHD) duct flow problems at

*Corresponding author. *Email addresses:* 952401001@cc.ncu.edu.tw (P.-W. Hsieh), yintzer_shih@email.nchu.edu.tw (Y. Shih), syyang@math.ncu.edu.tw (S.-Y. Yang)

high Hartmann numbers. We study the problem of finding the velocity u and the induced magnetic field b for a laminar, fully developed flow of an incompressible, viscous, electrically conducting fluid in a straight channel. The channel has a uniform cross-section Ω which is an open bounded region in $\mathbb{R}^2$ with a Lipschitz boundary $\partial\Omega$. The fluid is driven by a constant mechanical pressure gradient $-dp/dz$. The direction of the constant transverse external magnetic field b_0 may be arbitrary to the x-axis, and both the velocity u and the induced magnetic field b are parallel to the z-axis.

The generalized equations of the MHD duct flow described above with suitable boundary conditions can be posed in dimensionless form as follows [14,16]:

$$\begin{cases} -\varepsilon\Delta u+\boldsymbol{a}\cdot\nabla b=f_1, & \text{in } \Omega,\\ -\varepsilon\Delta b+\boldsymbol{a}\cdot\nabla u=f_2, & \text{in } \Omega,\\ u=g_1, & \text{on } \partial\Omega,\\ b=g_2, & \text{on } \Gamma_D,\\ \nabla b\cdot\boldsymbol{n}=g_3, & \text{on } \Gamma_N, \end{cases} \tag{1.1}$$

where $u=u(x,y)$ and $b=b(x,y)$ are the velocity and the induced magnetic field in the z-direction, respectively; ε is the diffusivity coefficient with $0<\varepsilon:=1/Ha<1$ and $Ha:=b_0 l\sqrt{\delta/\mu}$ is the Hartmann number, b_0 is the intensity of the external magnetic field, l is the characteristic length of the duct, δ and μ are the electric conductivity and coefficient of viscosity of the fluid respectively; the convection field is given by

$$\boldsymbol{a}:=(a_1,a_2)^\top=(-\sin\alpha,-\cos\alpha)^\top,$$

$\alpha\in[0,\pi/2]$ is the angle from the positive y-axis to the externally applied magnetic field b_0, measured in the clockwise direction; f_i for $i=1,2$ are the given source terms and in most practical MHD applications, we have

$$f_1\equiv\varepsilon \quad \text{or} \quad f_1\equiv 0 \quad \text{and} \quad f_2\equiv 0, \quad \text{in} \quad \Omega,$$

g_i for $i=1,2,3$ are prescribed boundary data;

$$\partial\Omega=\Gamma_D\cup\Gamma_N \quad \text{with} \quad \Gamma_D\cap\Gamma_N=\varnothing \quad \text{and} \quad |\Gamma_D|>0;$$

$\boldsymbol{n}$ is the outward unit normal vector to Γ_N.

There are many investigations which use various numerical methods such as finite difference, finite element and boundary element methods to solve the MHD duct flow problems. We refer the reader to [8,12–14,16–18] and many references cited therein. However, when the Hartmann number Ha is large, such an MHD duct flow problem consists of a coupled system of convection-dominated convection-diffusion equations. It is well known that the solution of convection-dominated problems may exhibit localized phenomena such as boundary or interior layers, i.e., narrow regions where some derivative of solution rapidly changes. Most conventional numerical methods can not efficiently

solve the layer problems because they are lacking in either stability or accuracy [10, 11]. The common deficiency of the existing numerical methods for the MHD duct flow problems is that they produce accurate results in several configurations of interest, but the Hartmann number Ha cannot be increased more than about 10^2 (cf. [12, 13]). However, from a practical point of view, the important range of Ha in industrial applications is from 10^2 to 10^6, i.e., the diffusivity coefficient ε varies from 10^{-6} to 10^{-2}.

One of the most successful class of numerical methods for treating convection-dominated problems is the stabilized finite element methods [2]. The subject of stabilized finite element methods has been intensively studied for more than twenty years, and it is still attractive today (see the recent review by Franca et al. [3] and many references cited therein). Moreover, the residual-free bubble method (cf. [1]) which is a stabilized-like finite element method has been demonstrated to be efficient for convection-dominated problems. Recently, Nesliturk and Tezer-Sezgin [12, 13] showed that the stabilized finite element method using the residual-free bubbles seems robust in MHD duct flow problems at high Hartmann numbers. In our recent work [8], we have devised a novel least-squares finite element method stabilized with the residual-free bubble functions for approximating the solution of MHD duct flow problem (1.1), which is reformulated as a first-order system by introducing two additional variables. One of the most distinguished features of this bubble-stabilized least-squares approach is that the resulting global linear system is symmetric and positive definite. However, the numerical results produced by these two bubble-stabilized methods still exhibit some spurious oscillations near the boundary layer regions when the Hartmann number Ha is large (cf. [8, 12, 13], see also Fig. 11 later).

In 2008, Han, Huang and Kellogg [6] proposed a tailored finite point method (henceforth, TFPM) for the numerical solution of a kind of homogeneous singular perturbation problems in unbounded domains. Using the artificial boundary method, the original problem is approximated by a convection-dominated convection-diffusion problem on a bounded domain. Then the TFPM uses special solutions of the homogeneous differential equation to construct an approximating discrete equation. The coefficients of the discrete equation are tailored to the special solutions of the homogeneous governing equation. This approach shows remarkable numerical results. Consequently, the Hemker Prize was awarded to them in the conference BAIL 2008 for their contribution to the goal of designing the best computational algorithm for the Hemker problem [7]. The TFPM they provided is well worth further study, both numerically on more complicated problems and analytically in an error analysis. Since then, the TFPM has been successfully applied to solve a class of linear singular perturbation problems with variable coefficients [5], the interface problems [9], and the convection-diffusion-reaction problems with a constant convection field [15]. More recently, several TFPMs are derived in [4] for solving the scalar inhomogeneous reaction-diffusion equations.

In this paper, we give a further study of the TFPM for solving steady MHD duct flow problems with a high Hartmann number. The problem under consideration consists of a coupled system of convection-dominated convection-diffusion equations. Firstly,

based on a similar idea to that used in [4] for treating the scalar inhomogeneous reaction-diffusion equations, we devise a tailored finite point method for the scalar inhomogeneous convection-diffusion equation, and then extend it to the MHD duct flow problem. For each interior grid point of a given rectangular mesh, we construct a finite-point difference operator at that point with some neighboring grid points, where the coefficients of the difference operator are tailored to some particular properties of the governing equations. We perform some numerical experiments on three examples to evaluate the effectiveness of the proposed TFPM. From the numerical results, one can find that the TFPM achieves very high accuracy with very coarse grid, even for very large Hartmann numbers. The theoretical error analysis of our method remains an open problem.

We now close this section with a brief remark. In [15], Shih, Kellogg and Tsai observed that, for obtaining accurate numerical results, the mesh grid points must be aligned with the convection field $\boldsymbol{a}$ when the TFPM is applied to solve the scalar convection-dominated problems with a sufficiently small ε. In this paper, we will give a heuristic explanation of why it is necessary, and propose a possible remedy to overcome the difficulty arising from this limitation. We also remark that if the diffusivity ε is not too small, then we do not need to require the grid points to be aligned with the convection field $\boldsymbol{a}$, see Example 4.1 in Section 4.

The remainder of this paper is organized as follows. In Section 2, we devise the tailored finite point method for the scalar inhomogeneous convection-diffusion equation, and then extend the method to the coupled system of convection-diffusion equations (1.1) in Section 3. In Section 4, several numerical examples are given to demonstrate the effectiveness of the proposed TFPM. Finally, in Section 5, some conclusions are made.

2 TFPM for the scalar inhomogeneous convection-diffusion problem

In this section, we derive the TFPM for the scalar inhomogeneous convection-diffusion equation,

$$-\varepsilon\Delta u+\boldsymbol{a}\cdot\nabla u=f, \quad \text{in } \Omega, \tag{2.1}$$

where $\boldsymbol{a}=(a_1,a_2)^\top$ with $|\boldsymbol{a}|=1$ is a given constant convection field and f is a given source function. Of course, this equation needs to be supplemented with some appropriate boundary condition.

Let $\mathcal{T}_h$ be a given rectangular mesh of domain Ω and let $p_0=(x_0,y_0)$ be an arbitrary chosen interior grid point. We take a small cell Ω_{p_0} centered at p_0 and surrounded by four nearby grid points $\{p_i=(x_i,y_i)\in\Omega,\ i=1,2,3,4\}$ (cf. Fig. 1, where the grid points are marked by the symbol $\bullet$). Considering (2.1) restricted on the cell Ω_{p_0} and approximating $f(x,y)$ in Ω_{p_0} by the constant $f(x_0,y_0)$, we have

$$-\varepsilon\Delta u+\boldsymbol{a}\cdot\nabla u=f(p_0), \quad \text{in } \Omega_{p_0}. \tag{2.2}$$

This is a reasonable approximation provided that the cell Ω_{p_0} is sufficiently small, i.e., h_1 and h_2 are small enough (cf. [4]). There are many other choices of approximations of $f(x,y)$ in Ω_{p_0} such as the average values

$$\frac{1}{5}\sum_{i=0}^{4} f(p_i) \quad \text{or} \quad \frac{1}{|\Omega_{p_0}|}\int_{\Omega_{p_0}} f(x,y)dxdy.$$

Now it is easy to verify that

$$\varphi_{p_0}(x,y) := f(p_0)(a_1 x + a_2 y) \tag{2.3}$$

is a solution of the inhomogeneous equation (2.2), namely,

$$-\varepsilon\Delta\varphi_{p_0} + \boldsymbol{a}\cdot\nabla\varphi_{p_0} = f(p_0), \quad \text{in } \Omega_{p_0}. \tag{2.4}$$

Letting $\widetilde{u} := u - \varphi_{p_0}$ in Ω_{p_0} and subtracting (2.4) from (2.2), we obtain the homogeneous equation,

$$-\varepsilon\Delta\widetilde{u} + \boldsymbol{a}\cdot\nabla\widetilde{u} = 0, \quad \text{in } \Omega_{p_0}. \tag{2.5}$$

We introduce a new variable $\widetilde{v}$ by

$$\widetilde{u}(x,y) := \exp\Big[\frac{a_1(x-x_0)+a_2(y-y_0)}{2\varepsilon}\Big]\widetilde{v}(x,y). \tag{2.6}$$

One can verify that $\widetilde{v}$ satisfies

$$-\varepsilon\exp\Big[\frac{a_1(x-x_0)+a_2(y-y_0)}{2\varepsilon}\Big]\Delta\widetilde{v} + \frac{1}{4\varepsilon}\exp\Big[\frac{a_1(x-x_0)+a_2(y-y_0)}{2\varepsilon}\Big]\widetilde{v} = 0, \quad in\Omega_{p_0},$$

and it leads to

$$\Delta\widetilde{v} - \kappa^2\widetilde{v} = 0, \quad \text{in } \Omega_{p_0}, \tag{2.7}$$

where $\kappa = 1/(2\varepsilon)$. We then convert (2.7) into the following form through the polar coordinate transformations, $x = x_0 + r\cos\theta$ and $y = y_0 + r\sin\theta$:

$$\widetilde{v}_{rr} + \frac{1}{r}\widetilde{v}_r + \frac{1}{r^2}\widetilde{v}_{\theta\theta} - \kappa^2\widetilde{v} = 0. \tag{2.8}$$

Now the general solution of Eq. (2.8) can be found by using the separation of variables. Suppose that $\widetilde{v}(r,\theta) = R(r)Q(\theta)$. Substituting it into (2.8), we get

$$R''(r)Q(\theta) + \frac{1}{r}R'(r)Q(\theta) + \frac{1}{r^2}R(r)Q''(\theta) - \kappa^2 R(r)Q(\theta) = 0. \tag{2.9}$$

By the techniques of separation of variables, we obtain for $n = 0,1,2,\cdots$,

$$Q''(\theta) + n^2 Q(\theta) = 0, \tag{2.10}$$

$$\overline{r}^2 R''(\overline{r}) + \overline{r}R'(\overline{r}) - (n^2 + \overline{r}^2)R(\overline{r}) = 0, \tag{2.11}$$

where $\overline{r}:=\kappa r$. Obviously, the general solution of (2.10) has the form

$$Q(\theta)=C_1\cos(n\theta)+C_2\sin(n\theta),$$

where $C_1,C_2\in\mathbb{R}$. On the other hand, Eq. (2.11) is the so-called modified Bessel differential equation and its solutions are the modified Bessel functions of the first kind, $I_n(\kappa r)$ for $n=0,1,2,\cdots$. Note that here we exclude the modified Bessel functions of the second kind $K_n(\kappa r)$, which solve the modified Bessel equation (2.11) as well, because $K_n(\kappa r)$ becomes infinite as r approaches zero. To sum up, the general solution of (2.8) can be formally expressed as

$$\widetilde{v}(r,\theta)=\xi_0 I_0(\kappa r)+\sum_{n=1}^{\infty}\Big(\xi_n I_n(\kappa r)\cos(n\theta)+\eta_n I_n(\kappa r)\sin(n\theta)\Big), \tag{2.12}$$

where $\xi_i,\eta_i\in\mathbb{R}$. According to (2.6), the general solution of (2.5) has the following form:

$$\widetilde{u}(r,\theta)=e^{\nu}\Big\{\xi_0 I_0(\kappa r)+\sum_{n=1}^{\infty}\Big(\xi_n I_n(\kappa r)\cos(n\theta)+\eta_n I_n(\kappa r)\sin(n\theta)\Big)\Big\},$$

where

$$\nu:=\frac{a_1 r\cos\theta+a_2 r\sin\theta}{2\varepsilon}.$$

Besides, one can easily find that every constant function $\widetilde{u}=C$ is also a solution of (2.5), and these constant solutions may be represented by the above infinite series with some specific coefficients. Thus, for later use, we rewrite the general form of $\widetilde{u}(r,\theta)$ as

$$\widetilde{u}(r,\theta)=\eta_0+e^{\nu}\Big\{\xi_0 I_0(\kappa r)+\sum_{n=1}^{\infty}\Big(\xi_n I_n(\kappa r)\cos(n\theta)+\eta_n I_n(\kappa r)\sin(n\theta)\Big)\Big\}, \tag{2.13}$$

where $\xi_i,\eta_i\in\mathbb{R}$.

We now introduce a tailored five-point method to approximate $\widetilde{u}(r,\theta)$. Firstly we define

$$\begin{aligned}&\Phi_1(r,\theta)=1, && \Phi_2(r,\theta)=e^{\nu}I_0(\kappa r),\\ &\Phi_3(r,\theta)=e^{\nu}I_1(\kappa r)\cos\theta, && \Phi_4(r,\theta)=e^{\nu}I_1(\kappa r)\sin\theta,\end{aligned}$$

and then construct the following 4-dimensional function space

$$\mathbf{W}:=\mathrm{span}\{\Phi_1,\Phi_2,\Phi_3,\Phi_4\}.$$

One can easily check that these functions Φ_i are solutions of (2.5). Let

$$\widetilde{u}_i:=u_i-\varphi_{p_0}(p_i)$$

denote the approximation of

$$\widetilde{u}(p_i)=u(p_i)-\varphi_{p_0}(p_i).$$

Then the tailored five-point approximations to (2.5), or equivalently (2.2), at the center $p_0=(x_0,y_0)$ are given by

$$\alpha_0\widetilde{u}_0+\alpha_1\widetilde{u}_1+\alpha_2\widetilde{u}_2+\alpha_3\widetilde{u}_3+\alpha_4\widetilde{u}_4=0. \tag{2.14}$$

That is, we have

$$\begin{aligned}&\alpha_0(u_0-\varphi_{p_0}(p_0))+\alpha_1(u_1-\varphi_{p_0}(p_1))+\alpha_2(u_2-\varphi_{p_0}(p_2))\\&+\alpha_3(u_3-\varphi_{p_0}(p_3))+\alpha_4(u_4-\varphi_{p_0}(p_4))=0,\end{aligned}$$

or written in the compact form

$$\sum_{i=0}^{4}\alpha_i u_i=\sum_{i=0}^{4}\alpha_i\varphi_{p_0}(p_i), \tag{2.15}$$

where the coefficients α_i ($i=0,1,2,3,4$) are obtained by solving the following underdetermined linear system

$$\alpha_0\Phi_j(p_0)+\alpha_1\Phi_j(p_1)+\alpha_2\Phi_j(p_2)+\alpha_3\Phi_j(p_3)+\alpha_4\Phi_j(p_4)=0, \tag{2.16}$$

for $j=1,2,3,4$.

Later we will explain how to solve the linear system (2.16) for the unknowns α_i with two different types of five-point stencil. By applying the tailored five-point formula (2.15) to each interior grid point in the given rectangular mesh $\mathcal{T}_h$, we obtain a global linear system of equations, where the boundary conditions are imposed as in the conventional finite difference schemes. Solving this global linear system will give us u_i's, which are the approximations to the exact values of the solution u of (2.1) at the grid points.

Now let us return to solve the algebraic system (2.16) for α_i's. Firstly we recall that the convection field is given by

$$\boldsymbol{a}:=(a_1,a_2)^\top,\quad \text{with}\quad a_1^2+a_2^2=1.$$

We define the so-called flow angle Θ of the convection field $\boldsymbol{a}$ by the angle between the vector $\boldsymbol{a}$ and the positive x-axis measured in counterclockwise direction. Thus, we always have $0\le\Theta<2\pi$. It has been suggested in [15] that in order to obtain accurate numerical solutions to convection-dominated convection-diffusion problems with a sufficiently small ε by using the TFPM, the mesh grid points must be aligned with the convection field $\boldsymbol{a}$. We will give a heuristic explanation of why it is necessary, and propose a possible remedy to overcome the difficulty arising from this limitation of the TFPM later in Remark 2.1.

We consider two five-point stencils depicted in Fig. 1. If we have a scalar convection-diffusion problem with a flow angle

$$\Theta\in\Big\{0,\frac{\pi}{2},\pi,\frac{3\pi}{2}\Big\},$$

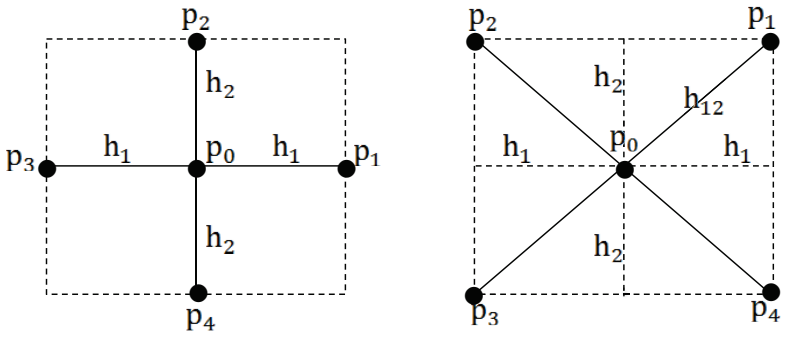

Figure 1: Five-point stencils of the TFPM: (left) type I; (right) type II.

then we should adopt a rectangular mesh with the five-point stencil of type I (this is what we mean " the grid points aligned with the convection field $\boldsymbol{a}$"); otherwise, we should use a mesh with the five-point stencil of type II, where the mesh sizes h_1 and h_2 are chosen so that the grid points aligned with the convection field $\boldsymbol{a}$.

2.1 The five-point stencil of type I

For convenience's sake, we define some notations as follows:

$$\nu_1=\frac{a_1h_1}{2\varepsilon},\quad \nu_2=\frac{a_2h_2}{2\varepsilon},\quad \tau_1=\frac{h_1}{2\varepsilon}\quad\text{and}\quad \tau_2=\frac{h_2}{2\varepsilon}.$$

By using type I stencil, the system of Eq. (2.16) can be expressed as

$$\begin{cases}\alpha_1+\alpha_2+\alpha_3+\alpha_4=-\alpha_0,\\ e^{\nu_1}I_0(\tau_1)\alpha_1+e^{\nu_2}I_0(\tau_2)\alpha_2+e^{-\nu_1}I_0(\tau_1)\alpha_3+e^{-\nu_2}I_0(\tau_2)\alpha_4=-\alpha_0,\\ e^{\nu_1}I_1(\tau_1)\alpha_1-e^{-\nu_1}I_1(\tau_1)\alpha_3=0,\\ e^{\nu_2}I_1(\tau_2)\alpha_2-e^{-\nu_2}I_1(\tau_2)\alpha_4=0.\end{cases}\tag{2.17}$$

Direct calculations imply that

$$\begin{cases}\alpha_1=\dfrac{1}{2K}e^{-\nu_1}\big(\cosh(\nu_2)-I_0(\tau_2)\big)\alpha_0,\\ \alpha_2=\dfrac{1}{2K}e^{-\nu_2}\big(I_0(\tau_1)-\cosh(\nu_1)\big)\alpha_0,\\ \alpha_3=\dfrac{1}{2K}e^{\nu_1}\big(\cosh(\nu_2)-I_0(\tau_2)\big)\alpha_0,\\ \alpha_4=\dfrac{1}{2K}e^{\nu_2}\big(I_0(\tau_1)-\cosh(\nu_1)\big)\alpha_0,\end{cases}\tag{2.18}$$

where

$$K:=\cosh(\nu_1)I_0(\tau_2)-\cosh(\nu_2)I_0(\tau_1).$$

Notice that we leave the unknown $\alpha_0 \neq 0$ as a degree of freedom. Moreover, after some tedious calculations, we can prove that

$$\lim_{\varepsilon\to 0^+}(\alpha_1,\alpha_2,\alpha_3,\alpha_4)=\begin{cases}(0,0,-\alpha_0,0), & \text{if } \Theta=0,\\ (0,0,0,-\alpha_0), & \text{if } \Theta=\pi/2,\\ (-\alpha_0,0,0,0), & \text{if } \Theta=\pi,\\ (0,-\alpha_0,0,0), & \text{if } \Theta=3\pi/2.\end{cases} \tag{2.19}$$

2.2 The five-point stencil of type II

We first define and recall some basic notations,

$$h_{12}=\sqrt{h_1^2+h_2^2},\quad \tau_{12}=\frac{h_{12}}{2\varepsilon},\quad \nu_1=\frac{a_1h_1}{2\varepsilon}\quad\text{and}\quad \nu_2=\frac{a_2h_2}{2\varepsilon}.$$

By applying type II stencil to the system of Eq. (2.16), we obtain the following explicit form

$$\begin{cases}\alpha_1+\alpha_2+\alpha_3+\alpha_4=-\alpha_0,\\ e^{\nu_1+\nu_2}I_0(\tau_{12})\alpha_1+e^{-\nu_1+\nu_2}I_0(\tau_{12})\alpha_2+e^{-\nu_1-\nu_2}I_0(\tau_{12})\alpha_3+e^{\nu_1-\nu_2}I_0(\tau_{12})\alpha_4=-\alpha_0,\\ e^{\nu_1+\nu_2}I_1(\tau_{12})\alpha_1-e^{-\nu_1+\nu_2}I_1(\tau_{12})\alpha_2-e^{-\nu_1-\nu_2}I_1(\tau_{12})\alpha_3+e^{\nu_1-\nu_2}I_1(\tau_{12})\alpha_4=0,\\ e^{\nu_1+\nu_2}I_1(\tau_{12})\alpha_1+e^{-\nu_1+\nu_2}I_1(\tau_{12})\alpha_2-e^{-\nu_1-\nu_2}I_1(\tau_{12})\alpha_3-e^{\nu_1-\nu_2}I_1(\tau_{12})\alpha_4=0.\end{cases} \tag{2.20}$$

Solving system (2.20) in unknowns α_i, we obtain

$$\begin{cases}\alpha_1=\dfrac{1}{2L}e^{-\nu_1-\nu_2}\big(\cosh(\nu_1-\nu_2)-I_0(\tau_{12})\big)\alpha_0,\\ \alpha_2=\dfrac{1}{2L}e^{\nu_1-\nu_2}\big(I_0(\tau_{12})-\cosh(\nu_1+\nu_2)\big)\alpha_0,\\ \alpha_3=\dfrac{1}{2L}e^{\nu_1+\nu_2}\big(\cosh(\nu_1-\nu_2)-I_0(\tau_{12})\big)\alpha_0,\\ \alpha_4=\dfrac{1}{2L}e^{-\nu_1+\nu_2}\big(I_0(\tau_{12})-\cosh(\nu_1+\nu_2)\big)\alpha_0,\end{cases} \tag{2.21}$$

where

$$L:=\cosh(\nu_1+\nu_2)I_0(\tau_{12})-\cosh(\nu_1-\nu_2)I_0(\tau_{12}).$$

Again, we leave the unknown $\alpha_0 \neq 0$ as a degree of freedom. Furthermore, we can verify that

$$\lim_{\varepsilon\to 0^+}(\alpha_1,\alpha_2,\alpha_3,\alpha_4)=\begin{cases}(0,0,-\alpha_0,0), & \text{if } 0<\Theta<\pi/2,\\ (0,0,0,-\alpha_0), & \text{if } \pi/2<\Theta<\pi,\\ (-\alpha_0,0,0,0), & \text{if } \pi<\Theta<3\pi/2,\\ (0,-\alpha_0,0,0), & \text{if } 3\pi/2<\Theta<2\pi.\end{cases} \tag{2.22}$$

We remark that the limit equation (2.22) as well as the identity (2.21) are always true no matter whether the mesh sizes h_1 and h_2 are chosen such that $h_2/h_1=|\tan(\Theta)|$ or not.

Remark 2.1. We now give a heuristic explanation of why the mesh grid points must be aligned with the convection field $\boldsymbol{a}$ when the TFPM is applied to solve the convection-dominated convection-diffusion problems with a sufficiently small ε. For simplicity, let us consider Eq. (2.1) in the homogeneous case and simplify it with $\varepsilon=0$, i.e.,

$$\boldsymbol{a}\cdot\nabla u=0, \quad \text{in } \Omega.$$

Note that for this purely hyperbolic equation the boundary values are prescribed only on the inflow part

$$\partial\Omega_-:=\{(x,y)\in\partial\Omega:\ \boldsymbol{n}(x,y)\cdot\boldsymbol{a}<0\}.$$

We assume that the inflow boundary condition is given by

$$u(x,y)=g(x,y), \quad \text{for } (x,y)\in\partial\Omega_-.$$

By the theory of hyperbolic equations, solution u must be a constant along each characteristic which is a straight line lying in the domain Ω parallel with the convection field $\boldsymbol{a}$. The constant value of u along a given characteristic is given by $g(x_0,y_0)$, where (x_0,y_0) is the point that the characteristic intersects the inflow boundary part $\partial\Omega_-$. Now suppose that the flow angle Θ satisfies $0<\Theta<\pi/2$, but $h_2/h_1\neq\tan(\Theta)$ (cf. type II stencil in Fig. 1). From (2.22) and (2.15), we obtain $u_0=u_3$ (notice that $\varphi_{p_0}(x,y)\equiv 0$ for every interior point p_0). Unfortunately, this will be probably an inaccurate result because p_0 and p_3 are not located at the same characteristic and in most cases, u should have different values at p_0 and p_3, i.e., $u(p_0)\neq u(p_3)$. In contrast, if we require $h_2/h_1=\tan(\Theta)$ then p_0 and p_3 will belong to the same characteristic, which implies $u(p_0)=u(p_3)$.

However, for example, if Θ is very close to $\pi/2$, then the use of type II stencil with $h_2/h_1=\tan(\Theta)$ implies the mesh will be very singular, i.e., $h_1\approx 0$. In such case, we may approximate Θ by $\pi/2$ and then use type I stencil rather than type II stencil. Another possible remedy to overcome this drawback of the TFPM is the use of the curvilinear grids. That is, one may construct a non-rectangular mesh of Ω such that the grid points aligned with the characteristic lines.

Remark 2.2. We remark that the choice of particular solution φ_{p_0} to the inhomogeneous equation (2.2) is not unique. Another possible choice is given by

$$\psi_{p_0}(x,y):=f(p_0)(a_1(x-x_0)+a_2(y-y_0)).$$

In such case, we have

$$\psi_{p_0}(x,y)=\varphi_{p_0}(x,y)+C,$$

where

$$C:=-f(p_0)(a_1x_0+a_2y_0)$$

is a constant. Now, due to the first equations in (2.17) and (2.20), we have

$$\sum_{i=0}^{4}\alpha_i=0,$$

which implies

$$0=\sum_{i=0}^{4}\alpha_i u_i-\sum_{i=0}^{4}\alpha_i\psi_{p_0}(p_i)=\sum_{i=0}^{4}\alpha_i u_i-\sum_{i=0}^{4}\alpha_i\varphi_{p_0}(p_i).$$

That is, the resulting global linear system (2.15) of the TFPM using the particular solution ψ_{p_0} is same with that using φ_{p_0}.

3 TFPM for the MHD duct flow problem

In this section, we extend the TFPM derived in Section 2 for scalar inhomogeneous convection-diffusion problems to the MHD duct flow problem (1.1). We follow the notation in Section 2. Let $p_0=(x_0,y_0)$ be an arbitrary chosen interior grid point in a rectangular mesh $\mathcal{T}_h$ of Ω and let Ω_{p_0} be a small cell centered at p_0 and surrounded by four nearby grid points $p_i=(x_i,y_i)$, $i=1,2,3,4$. The system of governing equations of the MHD duct flow (1.1) restricted on Ω_{p_0} can be approximated by

$$\begin{cases} -\varepsilon\Delta u+\boldsymbol{a}\cdot\nabla b=f_1(p_0), & \text{in } \Omega_{p_0},\\ -\varepsilon\Delta b+\boldsymbol{a}\cdot\nabla u=f_2(p_0), & \text{in } \Omega_{p_0}, \end{cases} \tag{3.1}$$

provided the cell Ω_{p_0} is sufficiently small. We then choose a particular solution of system (3.1) by

$$\big(\varphi^u_{p_0}(x,y),\varphi^b_{p_0}(x,y)\big):=\big(f_2(p_0)(a_1x+a_2y),f_1(p_0)(a_1x+a_2y)\big). \tag{3.2}$$

Define

$$u^*(x,y):=u(x,y)-\varphi^u_{p_0}(x,y) \quad \text{and} \quad b^*(x,y):=b(x,y)-\varphi^b_{p_0}(x,y). \tag{3.3}$$

Then we obtain the following coupled system of homogeneous convection-diffusion equations:

$$\begin{cases} -\varepsilon\Delta u^*+\boldsymbol{a}\cdot\nabla b^*=0, & \text{in } \Omega_{p_0},\\ -\varepsilon\Delta b^*+\boldsymbol{a}\cdot\nabla u^*=0, & \text{in } \Omega_{p_0}. \end{cases} \tag{3.4}$$

Introducing two new variables $\widetilde{U}$ and $\widetilde{B}$ by

$$\widetilde{U}:=u^*+b^* \quad \text{and} \quad \widetilde{B}:=u^*-b^*, \tag{3.5}$$

we have

$$u^*=\frac{1}{2}(\widetilde{U}+\widetilde{B}) \quad \text{and} \quad b^*=\frac{1}{2}(\widetilde{U}-\widetilde{B}). \tag{3.6}$$

It follows from (3.4) and (3.5) that

$$-\varepsilon\Delta\widetilde{U}+\boldsymbol{a}\cdot\nabla\widetilde{U}=0, \quad \text{in } \Omega_{p_0}, \tag{3.7}$$

$$-\varepsilon\Delta\widetilde{B}-\boldsymbol{a}\cdot\nabla\widetilde{B}=0, \quad \text{in } \Omega_{p_0}. \tag{3.8}$$

Notice that both (3.7) and (3.8) are scalar homogeneous convection-diffusion equations and the TFPM (2.14) developed in Section 2 for Eq. (2.5) can be applied to (3.7) and (3.8) directly. Following the similar procedure in Section 2, we define

$$\begin{aligned}
&\Phi_1^+(r,\theta)=1, && \Phi_2^+(r,\theta)=e^{\nu}I_0(\kappa r),\\
&\Phi_3^+(r,\theta)=e^{\nu}I_1(\kappa r)\cos\theta, && \Phi_4^+(r,\theta)=e^{\nu}I_1(\kappa r)\sin\theta,\\
&\Phi_1^-(r,\theta)=1, && \Phi_2^-(r,\theta)=e^{-\nu}I_0(\kappa r),\\
&\Phi_3^-(r,\theta)=e^{-\nu}I_1(\kappa r)\cos\theta, && \Phi_4^-(r,\theta)=e^{-\nu}I_1(\kappa r)\sin\theta,
\end{aligned}$$

where

$$\nu:=\frac{a_1 r\cos\theta+a_2 r\sin\theta}{2\varepsilon},$$

and then construct the following two function spaces:

$$\mathbf{W}^+:=\text{span}\{\Phi_1^+,\Phi_2^+,\Phi_3^+,\Phi_4^+\}\quad\text{and}\quad\mathbf{W}^-:=\text{span}\{\Phi_1^-,\Phi_2^-,\Phi_3^-,\Phi_4^-\}.$$

Let $\widetilde{U}_i$ and $\widetilde{B}_i$ denote the approximations of $\widetilde{U}(p_i)$ and $\widetilde{B}(p_i)$, respectively. Then the tailored five-point approximations to (3.7) and (3.8) at the interior grid point $p_0=(x_0,y_0)$ are respectively given by

$$\alpha_0\widetilde{U}_0+\alpha_1\widetilde{U}_1+\alpha_2\widetilde{U}_2+\alpha_3\widetilde{U}_3+\alpha_4\widetilde{U}_4=0, \tag{3.9}$$

$$\beta_0\widetilde{B}_0+\beta_1\widetilde{B}_1+\beta_2\widetilde{B}_2+\beta_3\widetilde{B}_3+\beta_4\widetilde{B}_4=0, \tag{3.10}$$

where the coefficients α_i and β_i in (3.9) and (3.10) are required to satisfy the following underdetermined linear systems of equations, respectively:

$$\alpha_0\Phi_j^+(p_0)+\alpha_1\Phi_j^+(p_1)+\alpha_2\Phi_j^+(p_2)+\alpha_3\Phi_j^+(p_3)+\alpha_4\Phi_j^+(p_4)=0,\qquad j=1,2,3,4, \tag{3.11}$$

$$\beta_0\Phi_j^-(p_0)+\beta_1\Phi_j^-(p_1)+\beta_2\Phi_j^-(p_2)+\beta_3\Phi_j^-(p_3)+\beta_4\Phi_j^-(p_4)=0,\qquad j=1,2,3,4. \tag{3.12}$$

Due to (3.6), we define the approximations of $u^*(p_i)$ and $b^*(p_i)$ by

$$u_i^*:=\frac{1}{2}(\widetilde{U}_i+\widetilde{B}_i)\quad\text{and}\quad b_i^*:=\frac{1}{2}(\widetilde{U}_i-\widetilde{B}_i),$$

respectively. Then by (3.9) and (3.10) the tailored five-point approximation to system (3.4) at the interior grid point $p_0=(x_0,y_0)$ is defined by

$$\begin{cases}\displaystyle\sum_{i=0}^{4}\alpha_i u_i^*+\sum_{i=0}^{4}\alpha_i b_i^*=0,\\ \displaystyle\sum_{i=0}^{4}\beta_i u_i^*-\sum_{i=0}^{4}\beta_i b_i^*=0.\end{cases} \tag{3.13}$$

Now, according to (3.3), we define the approximations of $u(p_i)$ and $b(p_i)$ by

$$u_i:=u_i^*+\varphi_{p_0}^u(p_i)\quad\text{and}\quad b_i:=b_i^*+\varphi_{p_0}^b(p_i).$$

The tailored five-point approximation to system (3.1) at the interior grid point $p_0=(x_0,y_0)$ is then given by

$$\begin{cases} \sum_{i=0}^{4}\alpha_i u_i+\sum_{i=0}^{4}\alpha_i b_i=\sum_{i=0}^{4}\alpha_i\Big(\varphi^u_{p_0}(p_i)+\varphi^b_{p_0}(p_i)\Big), \\ \sum_{i=0}^{4}\beta_i u_i-\sum_{i=0}^{4}\beta_i b_i=\sum_{i=0}^{4}\beta_i\Big(\varphi^u_{p_0}(p_i)-\varphi^b_{p_0}(p_i)\Big). \end{cases} \tag{3.14}$$

By applying the tailored five-point formula (3.14) to each interior grid point in the given rectangular mesh $\mathcal{T}_h$, we obtain a global linear system of equations, where the boundary conditions are imposed as in the conventional finite difference schemes.

4 Numerical experiments

In this section, we will give three numerical examples to demonstrate the high performance of our tailored five-point method for the MHD duct flow problem (1.1). However, the exact solution is available only for the first. Thus, in the first example, we can calculate the exact errors of the numerical solutions and estimate the convergence rates with respect to the mesh size h. For all test problems, we take $\alpha_0=\beta_0>0$.

Example 4.1. (The 2D square-channel flow with an exact solution) By constructing an inhomogeneous problem with an exact solution, in this example, we will study the convergence behavior of the TFPM. We take the domain

$$\Omega=(0,1)\times(0,1),\quad \varepsilon=10^{-2},\quad \boldsymbol{a}=\Big(-\sin\Big(\frac{\pi}{3}\Big),-\cos\Big(\frac{\pi}{3}\Big)\Big)^\top=\Big(\frac{-\sqrt{3}}{2},-\frac{1}{2}\Big)^\top.$$

Thus, the externally applied magnetic field makes a positive angle $\alpha=\pi/3$ with the y-axis, see Fig. 2. Define

$$Q_1(x,y)=\Big\{\frac{x^2}{2a_1}+\frac{\varepsilon x}{a_1^2}+\Big(\frac{1}{2a_1}+\frac{\varepsilon}{a_1^2}\Big)\Big(\frac{1-e^{\frac{a_1x}{\varepsilon}}}{e^{\frac{a_1}{\varepsilon}}-1}\Big)\Big\}\Big\{\frac{y^2}{2a_2}+\frac{\varepsilon y}{a_2^2}+\Big(\frac{1}{2a_2}+\frac{\varepsilon}{a_2^2}\Big)\Big(\frac{1-e^{\frac{a_2y}{\varepsilon}}}{e^{\frac{a_2}{\varepsilon}}-1}\Big)\Big\},$$
$$Q_2(x,y)=\Big\{\frac{-x^2}{2a_1}+\frac{\varepsilon x}{a_1^2}+\Big(\frac{-1}{2a_1}+\frac{\varepsilon}{a_1^2}\Big)\Big(\frac{1-e^{-\frac{a_1x}{\varepsilon}}}{e^{-\frac{a_1}{\varepsilon}}-1}\Big)\Big\}\Big\{\frac{-y^2}{2a_2}+\frac{\varepsilon y}{a_2^2}+\Big(\frac{-1}{2a_2}+\frac{\varepsilon}{a_2^2}\Big)\Big(\frac{1-e^{-\frac{a_2y}{\varepsilon}}}{e^{-\frac{a_2}{\varepsilon}}-1}\Big)\Big\}.$$

We then assume that the exact solutions u and b of problem (1.1) are given by

$$u(x,y)=Q_1(x,y)+Q_2(x,y)\quad\text{and}\quad b(x,y)=Q_1(x,y)-Q_2(x,y).$$

Then $u=b=0$ on $\partial\Omega$. Substituting solutions u and b into (1.1), we can obtain the inhomogeneous source terms f_1 and f_2. Since the diffusivity $\varepsilon=10^{-2}$ is not too small, we apply the TFPM using type II stencil with $h_1=h_2=h$ for $h=1/10,1/20,1/40,1/80$ to solve problem (1.1). Notice that in this example, the mesh grid points do not align with the convection field $\boldsymbol{a}=(-\sqrt{3}/2,-1/2)^\top$.

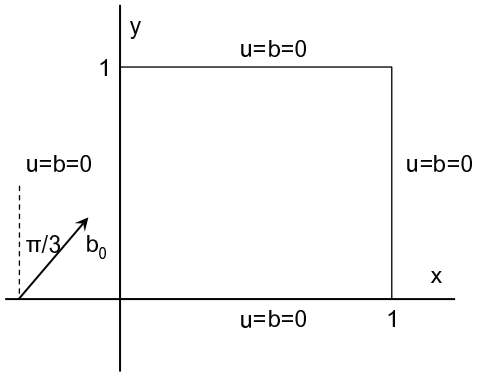

Figure 2: Problem statement of Example 4.1.

The elevation and contour plots of the exact solutions u and b and the approximate solutions u_h and b_h for $h=1/80$ are depicted in Figs. 3 and 4. One can observe that when the external magnetic field applies obliquely, the boundary layers are concentrated near the corners in the direction of the convection field for both solutions u and b. This is a well-known behavior of the MHD duct flows [8, 12]. The profiles of $u_h(x,0.1)$ and $b_h(x,0.9)$ for various mesh size h are shown in Fig. 5, where the exact errors of $u_h(0.1,0.1)$ and $b_h(0.9,0.9)$ are measured to estimate the rates of convergence of u_h and b_h with respect to the mesh size h. The rate of convergence of $u_h(0.1,0.1)$ is approximately 1.8742 and the rate of convergence of $b_h(0.9,0.9)$ is approximately 1.5489. Both convergence behavior are better than $\mathcal{O}(h^{1.5})$. From these numerical results, we can conclude that the TFPM produces stable and accurate results for this example.

Example 4.2. (The 2D square-channel flow with an oblique applied magnetic field) This is a frequently used test problem in the literature (cf. [12]). In this example, the domain is given by $\Omega:=(-1,1)\times(-1,1)$. The walls of the channel are insulated, i.e., $b=0$ on $\partial\Omega$, and the velocity is zero on the solid walls, i.e., $u=0$ on $\partial\Omega$. The right-hand side source functions in problem (1.1) are given by $f_1\equiv\varepsilon$ and $f_2\equiv 0$. That is, we still have an inhomogeneous MHD duct flow problem but with constant source functions. The externally applied magnetic field makes a positive angle α with the y-axis, see Fig. 6.

When $\alpha=\pi/2$ (i.e., $\boldsymbol{a}=(-1,0)^\top$ and the flow angle $\Theta=\pi$), we have the so-called Shercliff problem [12]. Although it is claimed in [12] that the problem possesses an analytic solution, only partial exact values of u and b for $\varepsilon=10^{-2}$ are available in [12]. In Table 1, we compare the absolute errors of the numerical solutions produced by the tailored five-point method using Type I stencil, the residual-free bubble method (RFBM) [12] and by the stabilized least-squares finite element method (LSFEM) [8], all using

$$h_1=h_2=\frac{1}{40},$$

with the exact values at the given specified grid points in the first quadrant of the channel.

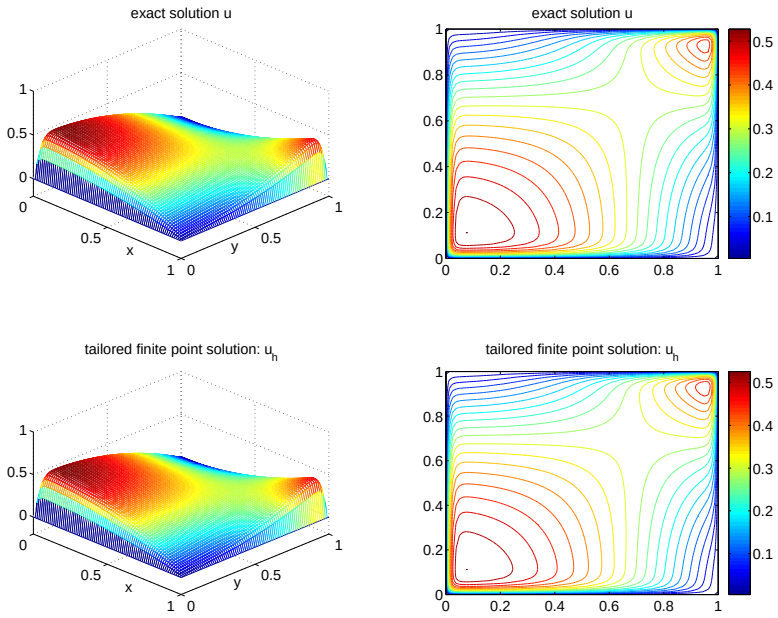

Figure 3: Exact solution u and tailored five-point solution u_h of Example 4.1 with $\varepsilon = 10^{-2}$ and $\boldsymbol{a} = (-\sqrt{3}/2, -1/2)^\top$ using type II stencil with $h_1 = h_2 = 1/80$.

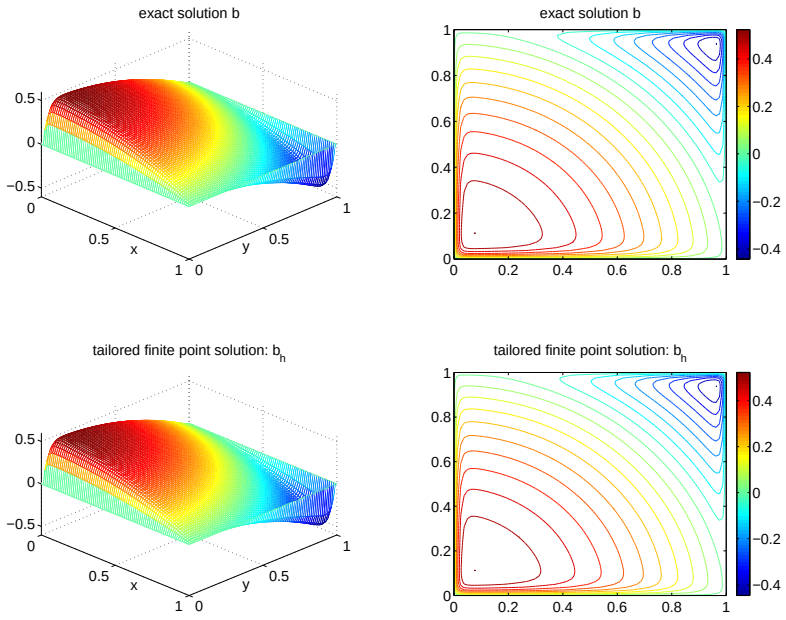

Figure 4: Exact solution b and tailored five-point solution b_h of Example 4.1 with $\varepsilon = 10^{-2}$ and $\boldsymbol{a} = (-\sqrt{3}/2, -1/2)^\top$ using type II stencil with $h_1 = h_2 = 1/80$.

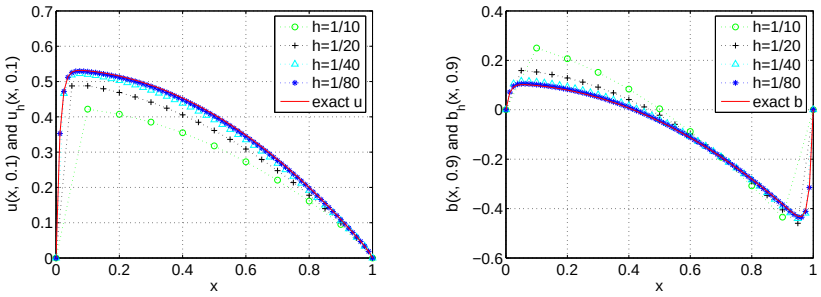

Figure 5: Profiles of $u_h(x,0.1)$ and $b_h(x,0.9)$ of Example 4.1 with $\varepsilon=10^{-2}$ and $\boldsymbol{a}=(-\sqrt{3}/2,-1/2)^\top$ using type II stencil with various $h(=h_1=h_2)$.

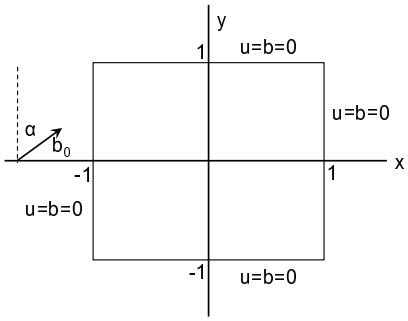

Figure 6: Problem statement of Example 4.2.

Table 1: A comparison of the absolute errors of numerical solutions of Shercliff's problem with $\varepsilon=10^{-2}$.

x	y	TFPM (u_h)	RFBM (u_h)	LSFEM (u_h)	TFPM (b_h)	RFBM (b_h)	LSFEM (b_h)
0.00	0.00	0	0	3.5150E-4	0	0	0
0.25	0.00	0	0	3.5330E-4	0	0	1.5200E-5
0.50	0.00	0	0	3.5860E-4	0	0	3.0600E-5
0.75	0.00	0	0	3.6680E-4	0	0	4.6200E-5
0.00	0.25	0	0	3.3740E-4	0	0	0
0.25	0.25	0	0	3.4060E-4	0	0	2.2400E-5
0.50	0.25	0	1.0000E-7	3.5000E-4	0	0	4.5100E-5
0.75	0.25	1.0000E-7	0	3.6480E-4	1.0000E-7	0	6.8100E-5
0.00	0.50	7.0000E-7	1.0000E-7	3.0140E-4	0	0	0
0.25	0.50	1.8000E-6	2.0000E-7	3.0930E-4	1.0000E-6	2.0000E-7	5.0800E-5
0.50	0.50	5.5000E-6	3.0000E-7	3.3280E-4	3.0000E-6	3.0000E-7	1.0040E-4
0.75	0.50	1.2300E-5	5.0000E-7	3.6930E-4	6.9000E-6	5.0000E-7	1.4750E-4
0.00	0.75	7.6800E-5	4.8000E-6	4.7760E-4	0	0	0
0.25	0.75	8.6400E-5	4.6000E-6	4.5480E-4	5.6600E-5	1.3000E-6	4.7400E-5
0.50	0.75	1.1460E-4	4.0000E-6	3.9210E-4	1.0890E-4	2.6000E-6	9.6600E-5
0.75	0.75	1.5730E-4	3.6000E-6	3.0750E-4	1.5720E-4	3.4000E-6	1.5720E-4

From the numerical results given in Table 1, it can be observed that all the methods exhibit acceptable results at the specified grid points when compared with the exact values.

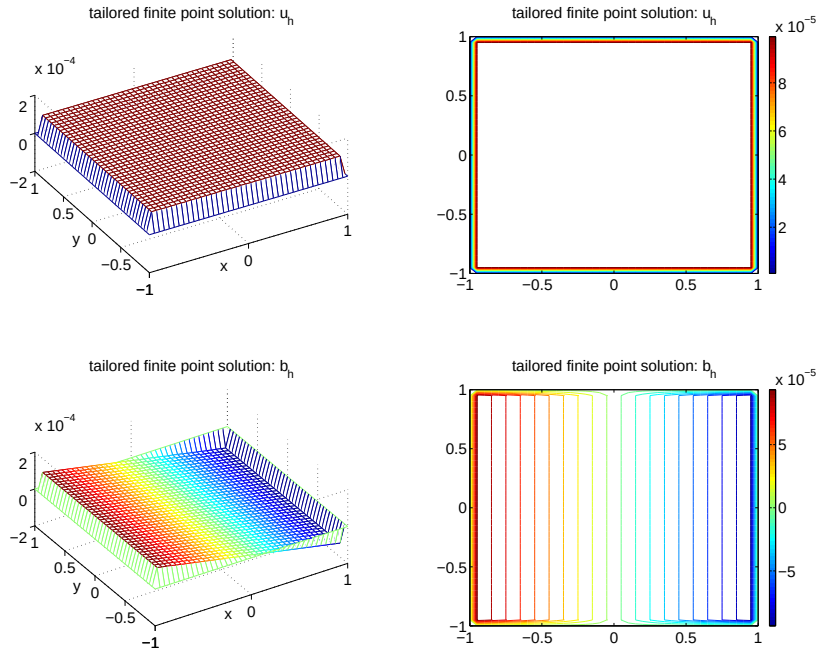

Figure 7: Numerical solutions of Example 4.2 with $\varepsilon=10^{-4}$ and $\alpha=\pi/2$ (i.e., $\boldsymbol{a}=(-1,0)^{\top}$) produced by the TFPM using type I stencil with $h_1=h_2=1/20$.

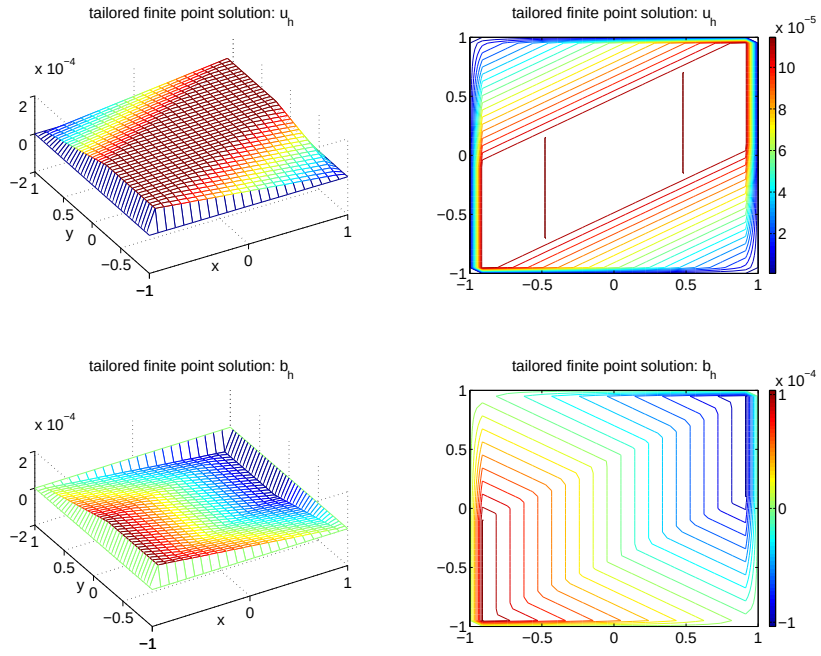

Figure 8: Numerical solutions of Example 4.2 with $\varepsilon=10^{-4}$ and $\alpha=\pi/3$ (i.e., $\boldsymbol{a}=(-\sqrt{3}/2,-1/2)^{\top}$) produced by the TFPM using type II stencil with $h_1=2/23$ and $h_2=1/20$.

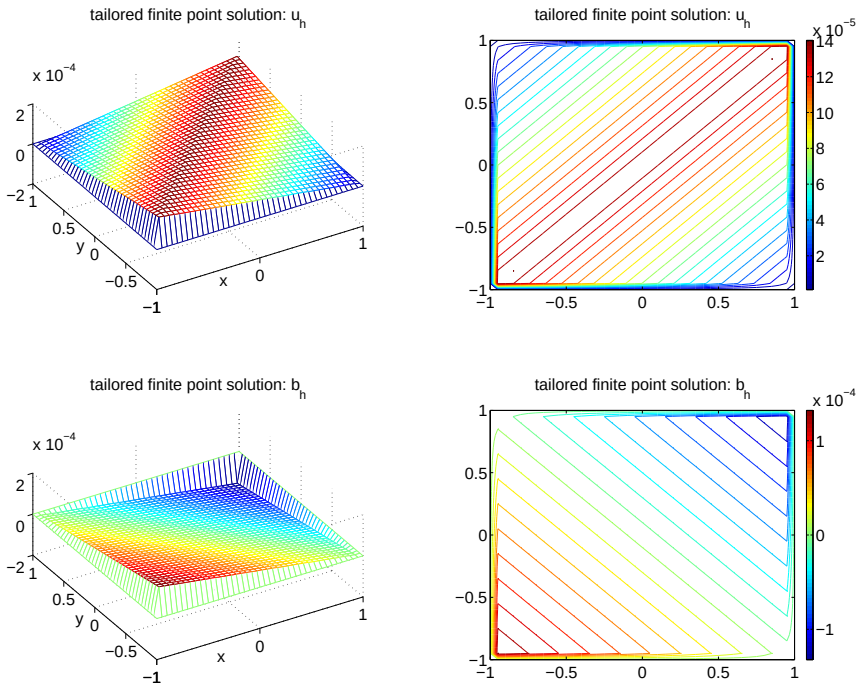

Figure 9: Numerical solutions of Example 4.2 with $\varepsilon=10^{-4}$ and $\alpha=\pi/4$ (i.e., $\boldsymbol{a}=(-\sqrt{2}/2,-\sqrt{2}/2)^{\top}$) produced by the TFPM using type II stencil with $h_1=h_2=1/20$.

In addition, it seems that RFBM gives better results than TFPM for $\varepsilon=10^{-2}$. However, when the diffusivity coefficient ε is getting small, the numerical solutions produced by the RFBM and the stabilized LSFEM will exhibit spurious oscillations near the boundary layer regions (e.g., see Fig. 11 given in Example 4.3). By contrast, the present TFPM always shows a high accuracy, even for a very small diffusivity coefficient ε.

Further computations for this example are carried out for $\varepsilon=10^{-4}$ and for values of $\alpha=\pi/2,\pi/3$ and $\pi/4$, where the corresponding flow angles are given by

$$\Theta=\pi,\ \frac{7\pi}{6}\ \text{and}\ \frac{5\pi}{4},$$

respectively. The elevation and contour plots for the approximate solutions generated by the TFPM are depicted in Figs. 7, 8 and 9. Apparently, when $\Theta=7\pi/6$ and $5\pi/4$, boundary layers appear near the corners,

$$(x,y)=(-1,-1)\quad\text{and}\quad(x,y)=(1,1).$$

Example 4.3. (The 2D square-channel flow driven by the current produced by electrodes [13]) We investigate the MHD flow in the 2D square-channel driven by the current produced by electrodes, placed one in each of the walls of the duct where the applied

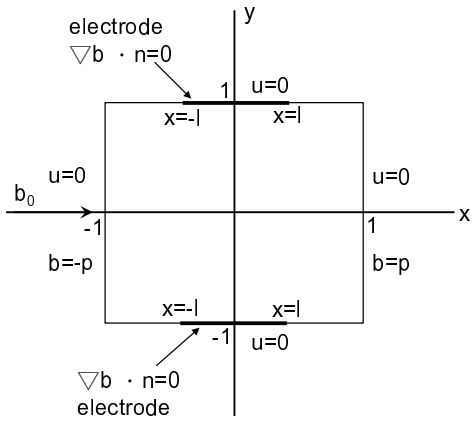

Figure 10: Problem statement of Example 4.3.

magnetic field b_0 is parallel, i.e., $\alpha=\pi/2$ (cf. Fig. 10). In this example, $f_i\equiv 0$ for $i=1,2$ and the boundary conditions are given by

$$\begin{cases} u=0, & \text{on } \partial\Omega, \\ b=p, & \text{on } \{(x,y)\in\partial\Omega: x>\ell,\ y=\pm 1\}\cup\{(x,y): x=1,\ -1\le y\le 1\}, \\ b=-p, & \text{on } \{(x,y)\in\partial\Omega: x<-\ell,\ y=\pm 1\}\cup\{(x,y): x=-1,\ -1\le y\le 1\}, \\ \nabla b\cdot\boldsymbol{n}=0, & \text{on } \{(x,y)\in\partial\Omega: -\ell\le x\le\ell,\ y=\pm 1\}. \end{cases}$$

In numerical computations, we set $\ell=0.3$ and $p=1$. We then consider the extreme case that $\varepsilon=10^{-6}$, i.e., we have an extremely large Hartmann number $Ha=10^6$.

Here, we impose the Neumann boundary conditions $\nabla b\cdot\boldsymbol{n}=0$ on the electrodes as in the conventional finite difference methods. For example, consider the type I stencil shown in Fig. 1. Suppose that b_0 and b_2 are the approximations of $b(p_0)$ and $b(p_2)$, respectively, and p_2 locates at the upper electrode. Since $\boldsymbol{n}(p_2)=(0,1)^\top$ and

$$0=\nabla b(p_2)\cdot\boldsymbol{n}(p_2)=\frac{\partial b}{\partial y}(p_2)\approx\frac{b(p_2)-b(p_0)}{h_2},$$

we require that $b_0=b_2$.

The elevation plots of the approximate solutions u_h and b_h produced by the TFPM using type I stencil with $h_1=h_2=1/20$ and by the bubble-stabilized LSFEM [8] with $h_1=h_2=1/40$ are displayed in Fig. 11. From these figures, it can be observed that boundary layer formation makes a strong appearance for u and b. The numerical results of the bubble-stabilized LSFEM still exhibit some spurious oscillations near the boundary layer regions. Similar phenomena occur in the numerical results of the RFBM [13]. In contrast, the TFPM presents a superior performance for such a high Hartmann number.

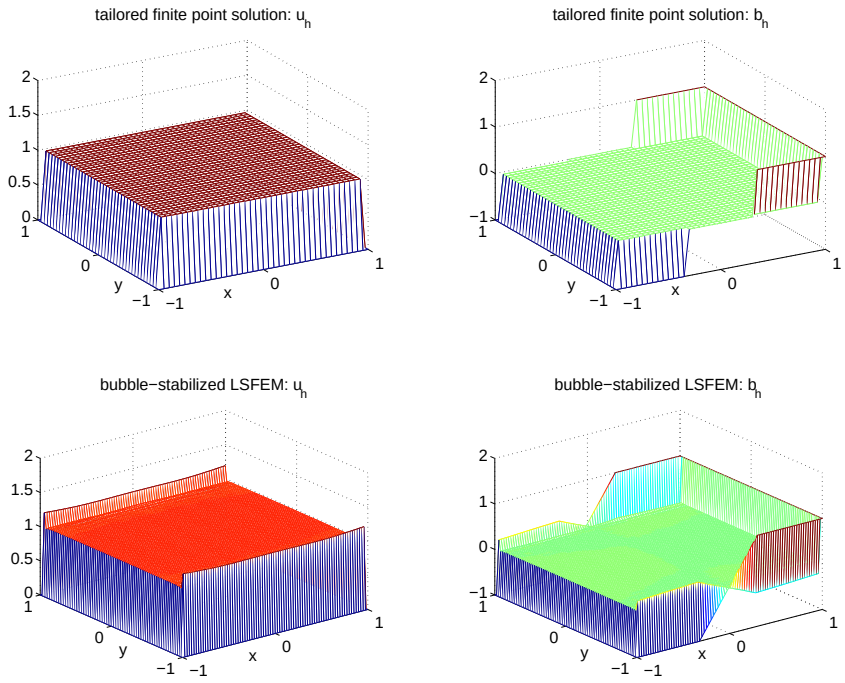

Figure 11: Numerical solutions of Example 4.3 with $\varepsilon=10^{-6}$ and $\alpha=\pi/2$ (i.e., $\boldsymbol{a}=(-1,0)^\top$) produced by the TFPM using type I stencil with $h_1=h_2=1/20$ and by the bubble-stabilized LSFEM with $h_1=h_2=1/40$.

5 Summary and conclusions

In this paper, we have proposed a TFPM for solving steady MHD duct flow problems with a high Hartmann number. Such an MHD duct flow is convection-dominated and the solution exhibits boundary layers. The presented TFPM is a development of the finite difference method. We first derive the tailored finite point method for the scalar inhomogeneous convection-diffusion equation, and then extend it to the MHD duct flow problem which consists of a coupled system of convection-diffusion equations. For each interior grid point of a given rectangular mesh, we construct a finite-point difference operator at that point with some neighboring grid points, where the coefficients of the difference operator are tailored to some particular properties of the problem. Finally, we have provided several numerical examples to illustrate the high performance of the proposed TFPM.

The most distinguished feature of this approach is that it can achieve very high accuracy with very coarse mesh even for very small ε. However, the disadvantage of this approach is that the mesh grid points must be aligned with the flow angle as $\varepsilon \ll 1$. Therefore, it should be a challenge when we deal with convection-dominated convection-diffusion problems with a variable convection field

$$\boldsymbol{a}(x,y)=(a_1(x,y),a_2(x,y))^\top.$$

A further study of the TFPM for solving coupled systems of inhomogeneous convection-dominated convection-diffusion equations with a variable convection field is under way.

Acknowledgments

The first and third authors would like to thank Prof. Thomas Y. Hou for bringing the work of Han-Huang-Kellogg [6] to their attention. The authors also would like to thank Prof. R. Bruce Kellogg and three anonymous referees for their valuable comments and suggestions on revising the paper. This work was supported by the National Science Council of Taiwan under the Grant NSC 97-2115-M-008-015-MY2.

References

[1] F. Brezzi and A. Russo, Choosing bubbles for advection-diffusion problems, Math. Mod. Meth. Appl. Sci., 4 (1994), 571–587.
[2] L. P. Franca, S. L. Frey and T. J. R. Hughes, Stabilized finite element methods: I. application to the advective-diffusive model, Comput. Method. Appl. Mech. Engrg., 95 (1992), 253–276.
[3] L. P. Franca, G. Hauke and A. Masud, Revisiting stabilized finite element methods for the advective-diffusive equation, Comput. Method. Appl. Mech. Engrg., 195 (2006), 1560–1572.
[4] H. Han and Z. Huang, Tailored finite point method for steady-state reaction-diffusion equation, Comm. Math. Sci., 8 (2010), 887–899.
[5] H. Han and Z. Huang, Tailored finite point method for a singular perturbation problem with variable coefficients in two dimensions, J. Sci. Comput., 41 (2009), 200–220.
[6] H. Han, Z. Huang and R. B. Kellogg, A tailored finite point method for a singular perturbation problem on an unbounded domain, J. Sci. Comput., 36 (2008), 243–261.
[7] H. Han, Z. Huang and R. B. Kellogg, The tailored finite point method and a problem of P. Hemker, Proceedings of the International Conference on Boundary and Interior Layers–Computaional and Asymptotic Methods, University of Limerick, Ireland, July 28-August 1, 2008.
[8] P.-W. Hsieh and S.-Y. Yang, A bubble-stabilized least-squares finite element method for steady MHD duct flow problems at high Hartmann numbers, J. Comput. Phys., 228 (2009), 8301–8320.
[9] Z. Huang, Tailored finite point method for the interface problem, Netw. Heterog. Media., 4 (2009), 91–106.
[10] K. W. Morton, Numerical Solution of Convection-Diffusion Problems, Chapman & Hall, London, UK, 1996.
[11] K. W. Morton and D. F. Mayers, Numerical Solution of Partial Differential Equations, Second Edition, Cambridge University Press, Cambridge, UK, 2005.
[12] A. I. Nesliturk and M. Tezer-Sezgin, The finite element method for MHD flow at high Hartmann numbers, Comput. Method. Appl. Mech. Engrg., 194 (2005), 1201–1224.
[13] A. I. Nesliturk and M. Tezer-Sezgin, Finite element method solution of electrically driven magnetohydrodynamic flow, J. Comp. Appl. Math., 192 (2006), 339–352.
[14] R. Scandiuzzi and B. A. Schrefler, FEM in steady MHD duct flow problems, Int. J. Numer. Meth. Engng., 30 (1990), 647–659.

[15] Y.-T. Shih, R. B. Kellogg and P.-S. Tsai, A tailored finite point method for convection-diffusion-reaction problems, J. Sci. Comput., 43 (2010), 239–260.
[16] B. Singh and J. Lal, Magnetohydrodynamic axial flow in a triangular pipe under transverse magnetic field, Indian J. Pure. Appl. Math., 9 (1978), 101–115.
[17] B. Singh and J. Lal, FEM in MHD channel flow problems, Int. J. Numer. Meth. Engng., 18 (1982), 1104–1111.
[18] B. Singh and J. Lal, FEM for unsteady MHD flow through pipes with arbitrary wall conductivity, Int. J. Numer. Meth. Fluids., 4 (1984), 291–302.